

However, from (A6), (A10), and (A12),

$$\|h_n\|_{N,2} < (B+2)^{1/2}/n; \quad (\text{A15})$$

and with  $n$  large enough, we have a contradiction between (A2) and (A14),

$$\int \chi(t)h_n(t)dt = 1 < A(B+2)^{1/2}/n. \quad (\text{A16})$$

Thus (A1) holds on  $H_{N,2}$  and therefore on  $\mathcal{D}_{L_2}$ .

Incidentally, note that this proof can be generalized to a distribution with arbitrary support. If  $\chi \in \mathcal{D}_{L_2}'$  with support  $K$ , then

$$\left| \int \chi(t)f(t)dt \right| \leq C \left\{ \sum_{l=0}^N \int_K |D^l f(t)|^2 dt \right\}^{1/2} \quad \text{for all } f \in \mathcal{D}_{L_2} \quad (\text{A17})$$

for some constants  $C$  and  $N$ .

## $K^+$ -Meson Branching-Ratio Measurement\*

M. E. ZELLER, R. P. HADDOCK, J. A. HELLAND,<sup>†</sup> AND J. PAHL  
*University of California, Los Angeles, California*

AND

N. T. DAIRIKI, R. L. BECK,<sup>‡</sup> K. M. CROWE, AND M. T. MAUNG<sup>§</sup>  
*Lawrence Radiation Laboratory, University of California, Berkeley, California 94720*  
(Received 24 October 1968)

A measurement of the rates  $K^+ \rightarrow \pi^0 + \pi^+$ ,  $K^+ \rightarrow \mu^+ \pi^0 \nu$ , and  $K^+ \rightarrow e^+ + \pi^0 + \nu$  with respect to  $K^+ \rightarrow \mu + \nu$  has been made by using a magnetic spectrometer and spark chambers. Both the range and momentum of the charged decay product are measured and compared with a Monte Carlo calculation. The decay in flight of the  $K^+$  mesons and the scattering of pions into the apparatus are rejected by a decay-time requirement. The results of the branching-ratio measurement are  $\Gamma(K_{\mu 2}) = (65.0 \pm 0.9)\%$ ,  $\Gamma(K_{\pi 2}) = (19.8 \pm 1.1)\%$ ,  $\Gamma(K_{\mu 3}) = (3.5 \pm 0.6)\%$ , and  $\Gamma(K_{e 3}) = (4.4 \pm 0.4)\%$ , on the assumptions  $\Gamma(\tau) = (5.57 \pm 0.03)\%$  and  $\Gamma(\tau') = (1.71 \pm 0.07)\%$ .

### I. INTRODUCTION

THE results of measurements of the branching ratios of the decay of the  $K^+$  meson, in particular the relative rates of

$$K^+ \rightarrow \pi^+ + \pi^0 \quad (K_{\pi 2}),$$

$$K^+ \rightarrow \mu^+ + \nu + \pi^0 \quad (K_{\mu 3}),$$

and 
$$K^+ \rightarrow e^+ + \nu + \pi^0 \quad (K_{e 3})$$

with respect to the mode  $K^+ \rightarrow \mu^+ + \nu$  ( $K_{\mu 2}$ ), are reported here. Table I and Fig. 1 show the results of previous measurements of these quantities.<sup>1-15</sup>

\* Work done under auspices of the U. S. Atomic Energy Commission.

<sup>†</sup> Present address: Department of Physics, University of Notre Dame, Notre Dame, Ind. 46556.

<sup>‡</sup> Present address: 1478 Ridge St., Redlands, Calif.

<sup>§</sup> Present address: Physics Department, University of California, San Diego, La Jolla, Calif.

<sup>1</sup> G. Alexander, R. H. W. Johnson, and C. O'Cealleigh, *Nuovo Cimento* **6**, 478 (1957).

<sup>2</sup> R. W. Birge, D. H. Perkins, J. E. Peterson, D. H. Stork, and M. N. Whitehead, *Nuovo Cimento* **4**, 834 (1959).

<sup>3</sup> S. Taylor, G. Harris, J. Orear, J. Lee, and P. Baumel, *Phys. Rev.* **114**, 359 (1959).

<sup>4</sup> B. P. Roe, D. Sinclair, J. L. Brown, D. A. Glaser, J. A. Kadyk, and G. H. Trilling, *Phys. Rev. Letters* **7**, 346 (1961).

<sup>5</sup> F. S. Shaklee, G. L. Jensen, B. P. Roe, and D. Sinclair, *Phys. Rev.* **136B**, 1423 (1964).

Prior to 1964, determinations of these branching ratios had been made by use of emulsions and heavy-liquid bubble chambers. Such measurements have two possible sources of systematic errors that limit the accuracy of the results: (a)  $K^+$  decay in flight, which

<sup>6</sup> G. Borreani, G. Rinaudo, and A. E. Werbrouck, *Phys. Letters* **12**, 123 (1964).

<sup>7</sup> V. Bisi, G. Borreani, R. Cester, A. DeMarco-Trabuco, M. T. Ferrero, C. M. Garelli, A. Marzari-Chiesa, B. Quassiat, G. Rinaudo, M. Vigone, and A. Werbrouck, *Nuovo Cimento* **35**, 768 (1965).

<sup>8</sup> A. Callahan and D. Cline, *Phys. Rev. Letters* **15**, 129 (1965).

<sup>9</sup> A. C. Callahan, U. Camerini, R. D. Hantman, R. H. March, D. L. Murphree, G. Gidal, G. E. Kalmus, W. M. Powell, C. L. Sandler, R. T. Pu, S. Natali, and M. Villani, *Phys. Rev.* **150**, 1153 (1966).

<sup>10</sup> G. H. Trilling, in *Proceedings of the Argonne International Conference on Weak Interactions, 1965* [Argonne National Laboratory Report No. ANL-7130 (unpublished)], pp. 115-149.

<sup>11</sup> L. B. Auerbach, J. MacG. Dobbs, A. K. Mann, W. K. McFarlane, D. H. White, R. Cester, P. T. Eschstruth, G. K. O'Neill, and D. Yount, *Phys. Rev.* **155**, 1505 (1967).

<sup>12</sup> R. L. Beck, University of California Lawrence Radiation Laboratory Report No. UCRL-16003, 1966 (unpublished).

<sup>13</sup> T. Eichten *et al.*, *Phys. Letters* **27B**, 586 (1968).

<sup>14</sup> R. Garland, K. Tsipis, S. Devons, J. Rosen, D. Tycko, L. G. Pondrom, and S. L. Meyer, *Phys. Rev.* **167**, 1225 (1968).

<sup>15</sup> D. R. Botterill, R. M. Brown, A. B. Clegg, I. F. Corbet, G. Culligan, J. McL. Emmerson, R. C. Field, J. Garvey, P. B. Jones, N. Middlemas, D. Newton, T. W. Quirk, G. L. Salmon, P. H. Steinberg, and W. S. C. Williams, *Phys. Rev. Letters* **21**, 766 (1968).

TABLE I. Results of previous measurements (branching ratios, in %).

Ref.	Experiment	$K^+ \rightarrow \mu^+ + \nu$ $K_{\mu 2}$	$K^+ \rightarrow \pi^+ + \pi^0$ $K_{\pi 2}$	$K^+ \rightarrow \mu^+ + \pi^0 + \nu$ $K_{\mu 3}$	$K^+ \rightarrow e^+ + \pi^0 + \nu$ $K_{e 3}$	$K_{\mu 3}/K_{e 3}$	$K^+ \rightarrow 2\pi^+ + \pi^-$ $\tau^+$	$K^+ \rightarrow \pi^+ + 2\pi^0$ $\tau^+$	Method
1	Alexander <i>et al.</i> , 1957	56.9 $\pm$ 2.6	23.2 $\pm$ 2.2	5.9 $\pm$ 1.3	5.1 $\pm$ 1.3	1.16 $\pm$ 0.39	6.8 $\pm$ 0.4	2.2 $\pm$ 0.4	Emulsion
2	Birge <i>et al.</i> , 1959	58.5 $\pm$ 3.0	27.7 $\pm$ 2.7	2.8 $\pm$ 1.0	3.2 $\pm$ 1.3	0.88 $\pm$ 0.47	5.6 $\pm$ 0.4	2.1 $\pm$ 0.5	Emulsion
3	Taylor, 1959			2.8 $\pm$ 0.4			5.2 $\pm$ 0.3	1.5 $\pm$ 0.2	Emulsion
4	Roe <i>et al.</i> , 1961	64.2 $\pm$ 1.3	18.6 $\pm$ 0.9	4.8 $\pm$ 0.6	5.0 $\pm$ 0.5	0.96 $\pm$ 0.15	5.7 $\pm$ 0.2	1.7 $\pm$ 0.2	Xe bubble chamber
5	Shaklee <i>et al.</i> , 1964	63.0 $\pm$ 0.8	22.4 $\pm$ 0.8	3.8 $\pm$ 0.5	4.7 $\pm$ 0.3	0.63 $\pm$ 0.10	5.1 $\pm$ 0.2	1.8 $\pm$ 0.2	Xe bubble chamber
6	Borreani, 1964				5.12 $\pm$ 0.36				H <sub>2</sub> bubble chamber
7	Bisi, 1965			3.45 $\pm$ 0.56					H <sub>2</sub> bubble chamber
									Propane freon bubble chamber
8	Callahan <i>et al.</i> , 1965		21.0 $\pm$ 0.56						Freon bubble chamber
9	Callahan <i>et al.</i> , 1965		21.0 $\pm$ 0.9	2.77 $\pm$ 0.19	3.94 $\pm$ 0.21	0.703 $\pm$ 0.056			(Summary)
10	Trilling, 1965	63.5 $\pm$ 0.7	21.6 $\pm$ 0.6	3.17 $\pm$ 0.35	4.49 $\pm$ 0.25	0.706 $\pm$ 0.087			Spectrometer and spark chambers
11	Auerbach <i>et al.</i> , 1967	63.34 $\pm$ 0.44	20.61 $\pm$ 0.32	3.81 $\pm$ 0.26	4.96 $\pm$ 0.13	0.767 $\pm$ 0.052			Spectrometer
12	Beck, 1967		$K_{\mu 2}/K_{\pi 2} = 2.31 \pm 0.24$						
13	ABC OPPVM Collab., 1968					0.604 $\pm$ 0.022			Bubble chamber
14	Garland <i>et al.</i> , 1968			3.5 $\pm$ 0.3	4.4 $\pm$ 0.4	0.80 $\pm$ 0.10			Spectrometer
15	Botterill <i>et al.</i> , 1968			3.29 $\pm$ 0.11	4.94 $\pm$ 0.11	0.667 $\pm$ 0.017			Spectrometer

confuses the separation of the  $K_{\mu 2}$  and  $K_{\pi 2}$  modes from the other modes, and (b) the energy dependence of the fiducial volume, which causes uncertainty in the number of detectable decays.

One of the objectives in the design of this experiment was to minimize these possible errors.

A second objective of the experiment was to obtain a more precise determination of the ratio  $\Gamma(K_{\pi 2})/\Gamma(K_{\mu 2})$ . There is presently no theoretical calculation of this ratio, but the previous experimental results are sufficiently scattered to warrant further investigation.

The hadron current describing the semileptonic three-body  $K$  decay involves two form factors  $f_+(q^2)$  and  $f_-(q^2)$  which are scalar functions of the square of the four-momentum transferred to the leptons  $q^2$ . Both the ratio of decay rates of these modes  $\Gamma(K_{\mu 3})/\Gamma(K_{e 3})$  and the muon polarization can be expressed as functions of the ratio  $\xi(q^2) = f_-(q^2)/f_+(q^2)$ . Present experimental evidence<sup>16,17</sup> indicates  $\xi(q^2)$  is real; however, previous experiments yield widely varying results for the value of  $\xi(q^2)$  as determined from branching ratios and measurements of  $K_{\mu 3}$  muon polarization.<sup>1-15,18-20</sup> Figure 2 shows these results. A purpose of this experiment was to investigate this discrepancy.

It has been suggested that an underestimate of the momentum-transfer dependence of the form factors  $f_+(q^2)$  and  $f_-(q^2)$  could be responsible for a misinterpretation of branching-ratio measurements of the semileptonic modes.<sup>21,22</sup> In calculating the effects of

strong  $q^2$  dependence, we find it has little effect on the momentum spectra of the charged lepton.<sup>23</sup> Thus, allowing for a large variation of the form factors does not bring the value of  $\xi$  as determined by a measurement of  $\Gamma(K_{\mu 3})/\Gamma(K_{e 3})$  into agreement with that of the polarization measurement.

The form factors can be expanded in powers of  $q^2/m_\pi^2$ . If the dependence on  $q^2$  is small, only the first term need be retained<sup>24</sup>:

$$f_\pm(q^2) = f_\pm(0)[1 + \lambda_\pm(q^2/m_\pi^2)].$$

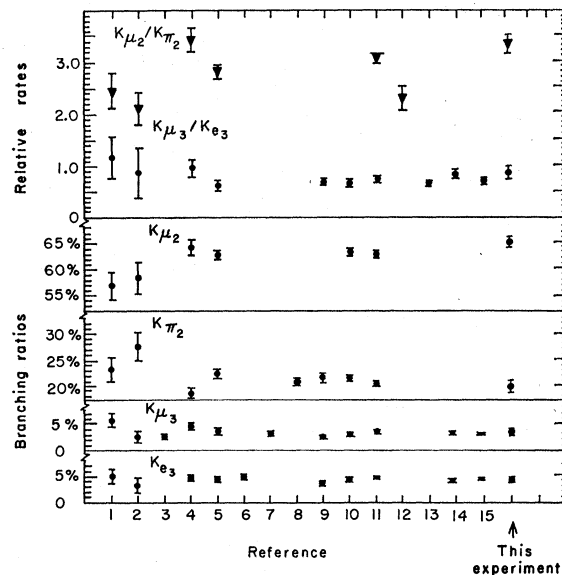


FIG. 1. Branching ratio of previous measurements.

<sup>16</sup> K. K. Young, M. J. Longo, and J. A. Helland, Phys. Rev. Letters **18**, 806 (1967).

<sup>17</sup> D. Bartlett, C. E. Freidberg, K. Goulianos, and D. Hutchinson, Phys. Rev. Letters **16**, 282 (1966).

<sup>18</sup> D. Cutts, M. Deutsch, R. Stiening, and C. Wiegand, Phys. Rev. Letters **20**, 955 (1968).

<sup>19</sup> J. Bettels *et al.*, Nuovo Cimento **56A**, 1106 (1968).

<sup>20</sup> L. B. Auerbach, A. K. Mann, W. K. McFarlane, and F. J. Sciulli, Phys. Rev. Letters **17**, 980 (1966).

<sup>21</sup> L. B. Auerbach, A. K. Mann, W. K. McFarlane, and F. J. Sciulli, Phys. Rev. Letters **19**, 464 (1967).

<sup>22</sup> B. d'Espagnat and M. K. Gaillard, Phys. Letters **25B**, 346 (1967).

<sup>23</sup> M. E. Zeller, UCLA Report No. 34P106-26, 1968 (unpublished).

<sup>24</sup> P. Dennery and H. Primakoff, Phys. Rev. **131**, 1334 (1963).

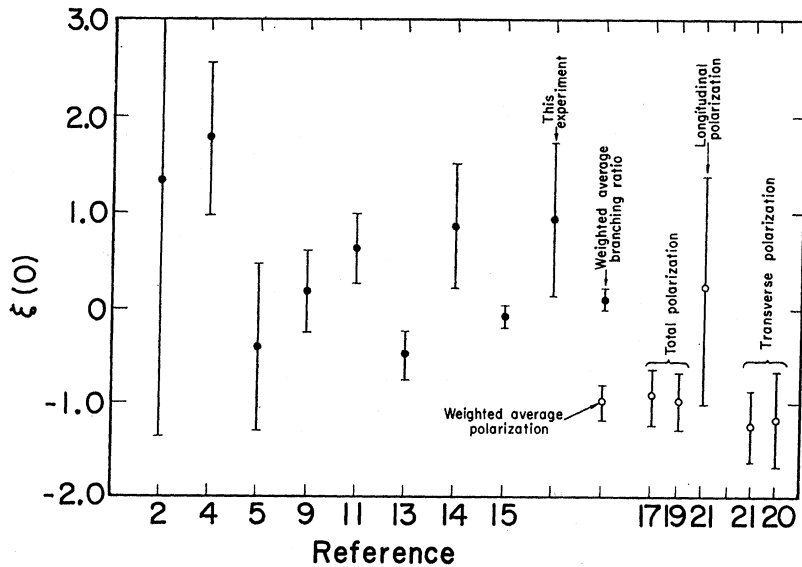


FIG. 2. Comparison of  $\xi(0)$  by branching ratio and polarization.

Previous experiments<sup>25</sup> have determined  $\lambda_+ = 0.023 \pm 0.008$ . As no precise measurement of  $\lambda_-$  has been made, we have assumed  $\lambda_- = 0$ .

In establishing the branching ratios, we have compared the data with theoretical predictions of the momentum spectra based on assumptions of local leptonic coupling, muon electron universality, and vector-axial-vector weak interactions.<sup>26</sup> The expression that is used in relating  $\xi$  to the measured branching ratios of the semileptonic modes was obtained by Cabibbo<sup>27</sup>:

$$\Gamma(K_{\mu 3})/\Gamma(K_{e 3}) = 0.6487 + 0.1045 M_{K^2} \lambda_+ / M_{\pi^2} + \text{Re}[\xi(0)](0.1269 + 0.006 \times M_{K^2} \lambda_+ / M_{\pi^2}) + |\xi(0)|^2(0.0193 - 0.0053 M_{K^2} \lambda_+ / M_{\pi^2}).$$

This equation was evaluated with  $\lambda_+ = 0.023$  and  $\xi(0) = f_-(q^2=0)/f_+(q^2=0)$ .<sup>28</sup>

## II. EXPERIMENTAL DETAILS

### A. Beam

$K^+$  mesons were produced from protons in the external proton beam of the Bevatron impinging on a platinum target. The target was 6.5 cm along the proton beam, 0.62 cm wide, and 0.95 cm high. Figure 3 shows the transport system for the  $K^+$  beam, 500 MeV/ $c \pm 5\%$ , from the production target to the  $K^+$  stopping region. This system produced a  $K^+$  image separated from the pions and protons by use of a separator with crossed electric and magnetic fields. It employed strong-focusing bending magnets ( $M2$  and  $M3$ ) to reduce the over-all

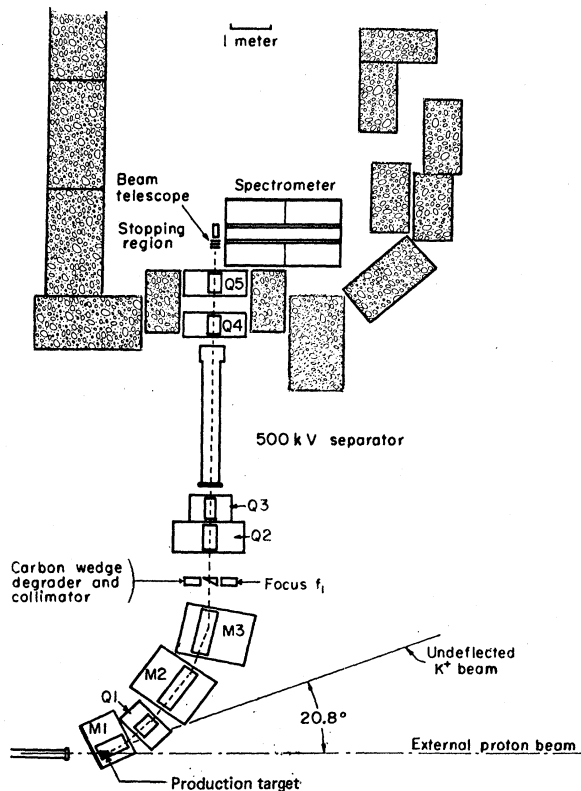


FIG. 3. Plan view of  $K^+$  beam arrangement.

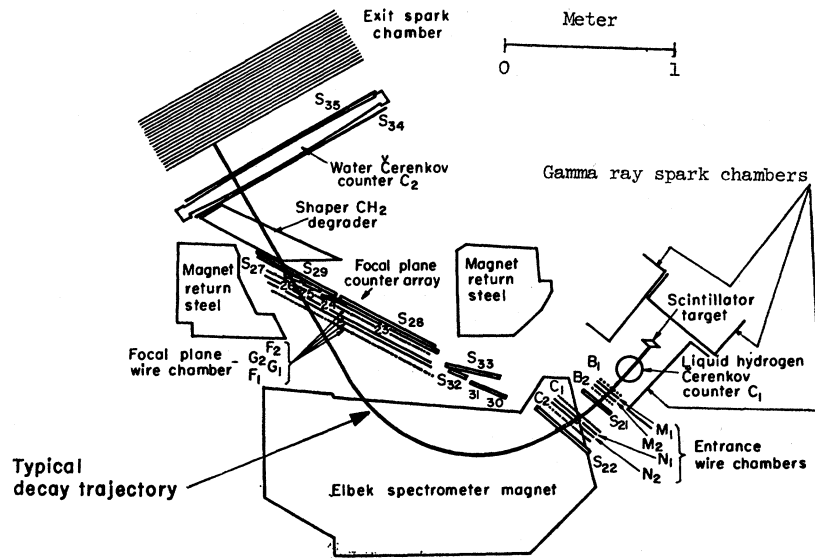
<sup>25</sup> W. J. Willis, Rapporteur talk, in *Proceedings of the Heidelberg International Conference on Elementary Particles*, edited by H. Filthuth (Wiley-Interscience, Inc., New York, 1968).

<sup>26</sup> N. Brene, L. Egdardt, and B. Qvist, *Nucl. Phys.* **22**, 553 (1961).

<sup>27</sup> N. Cabibbo, in *Proceedings of the Thirteenth International Conference on High-Energy Physics, Berkeley, 1966* (University of California Press, Berkeley, 1967), p. 29.

<sup>28</sup> The use of  $\lambda_+ = 0.023$  is a slight departure from the usual analysis for which  $\lambda_+$  is taken as 0.0 (Refs. 1-12). The difference in the determination of  $\xi(q^2)$  from the previous evaluations is a reduction of  $\xi$  by approximately 5%. The values of  $\xi(q^2)$  in Fig. 2 have all been evaluated with  $\lambda_+ = 0.023$  and the respective experimentally determined branching ratios.

FIG. 4. Schematic drawing of Elbek spectrometer and detection apparatus (the  $K^+$ 's enter the scintillator target in a direction out of the plane of the paper).



length of the flight path while retaining the focusing properties of a quadrupole system.

The momentum spread at the stopping target was reduced to  $\pm 2\%$  by means of a wedge-shaped carbon degrader placed at the first focus. The angular acceptance from the production target was 5 msr, and the image size at the stopping target was 2.5 cm horizontally and 1.8 cm vertically. The vertical separation between  $K^+$ 's and protons was 6.1 cm, and between  $K^+$ 's and pions 2.1 cm. Approximately 3000  $K^+$  mesons were transmitted to the stopping target per Bevatron pulse of  $5 \times 10^{11}$  protons incident on the production target, and of these, 800 were stopped.

### B. Apparatus

Figure 4 shows a schematic drawing of the apparatus, including a typical  $K$ -decay particle trajectory. The directions and positions of an orbit were determined by twelve wire spark chambers placed at the entrance and exit of the spectrometer. The spectrometer was designed so that rays leaving the center of the target would focus on a plane approximately coincident with the  $F1$  wire chamber, independent of their initial angle.<sup>29</sup> The position along this focal plane of the image of such a point source is determined only by the momentum of the particles and the dispersion of the spectrometer, approximately  $0.85 \text{ cm}/(\text{MeV}/c)$ . Another property of the spectrometer is that rays of different momentum leaving the center of the target along the optic axis all exit from the magnet parallel to one another. The momentum acceptance of the spectrometer is from 120 to  $235 \text{ MeV}/c$ .

Leaving the spectrometer, a particle continued on until it stopped in a spark chamber with twenty

$0.635\text{-cm}$  aluminum plates (exit chamber). A wedge-shaped polyethylene degrader was placed between the exit of the spectrometer and the spark chamber so that the higher-momentum muons from  $K_{\mu 2}$  would stop in the exit chamber.

An event trigger was formed by a delayed coincidence between the stopping  $K^+$  telescope, the decay telescope formed by  $S_{21}$  and  $S_{22}$ , and a pair of scintillation counters at the focal plane. The time between a stopping  $K^+$  event and the subsequent decay product that passed through counter  $S_{21}$  and  $S_{22}$  was recorded with a time-to-height converter system, and this information was used to reject events in which the  $K^+$  decayed in flight.

Surrounding the  $K^+$  stopping region was a set of three spark chambers with brass plates. These chambers were designed to detect the  $\gamma$  rays resulting from  $\pi^0$  meson decay, and were not used in the aspect of the experiment herein reported.

### C. Efficiency Measurements and Calibration

The efficiency of the focal-plane wire spark chambers was measured by extrapolating tracks observed in the exit spark chamber back to the focal plane. The ratio

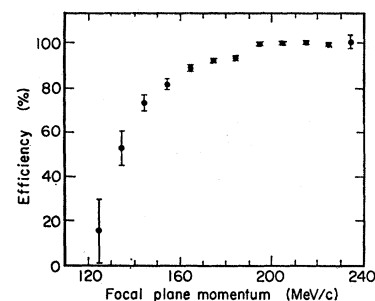


FIG. 5. Focal-plane wire chamber efficiency as a function of momentum.

<sup>29</sup> J. Borggreen, B. Elbek, and L. Perch Nielsen, Nucl. Instr. Methods 24, 1 (1963).

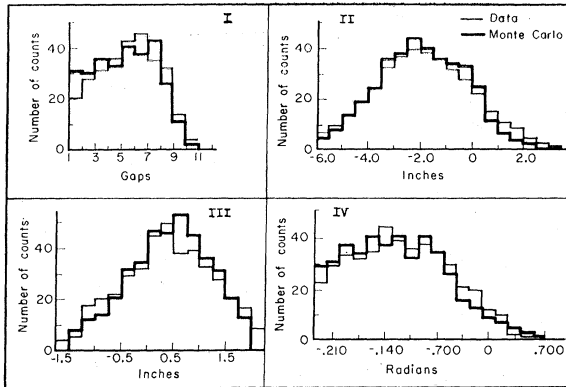


FIG. 6. Comparison of data and Monte Carlo calculations. (I) Distribution of penetration into the exit chamber of muons from  $K_{\mu 2}$ . (II) Deviation of actual spark location in the exit chamber from projected positions. (III) Initial spatial distribution of events. (IV) Initial angular distribution of events.

of the number of recorded wire chamber tracks to the total number of tracks then gave the efficiency as a function of position or momentum at the focal plane; the efficiency is shown in Fig. 5. The efficiency of the exit chamber was measured at the Berkeley 184-in. cyclotron and found to be  $(95 \pm 2)\%$  efficient, independent of particle type or position in the chamber.

The spectrometer field was measured and fitted with simple polynomials to an accuracy of approximately 1%. This representation of the field was used in a computer program that simulated particle trajectories through the system. The accuracy of the orbit-tracking calculation was checked in two ways: (a) comparison with floating-wire measurements, and (b) comparison between prediction and actual position of the  $K_{\mu 2}$  and  $K_{\pi 2}$  momentum peaks. In the first method the program predicted wire trajectories to an accuracy of approximately 2 mm at any point along the wire. This uncertainty was included in the final analysis. The second check on the reliability of the program is discussed in Sec. III.

#### D. Data Collection and Reduction

A PDP-5 Digital Equipment Corp. on-line computer was used to monitor the data-taking process as well as to record the data on magnetic tape. Recorded data consisted of counter, wire chamber, and time-of-flight information for each event. In addition, both a Vidicon system and a film camera were employed to digitize and record the spark positions of particle tracks in the exit spark chamber.

A data-reduction program correlated the spark information into recognizable tracks, thinned the wire chamber data, and merged the information on one tape with the counter data for each event. The wire chamber thinning involved the averaging of adjacent wire addresses and recording these averaged addresses as well as the number of wires averaged. The points at

which the particle trajectory crossed the wire chambers were used to reconstruct the momentum and initial position and direction of each event. The particle range was calculated from the focal plane to the stopping point in the exit spark chamber.

As a measure of the quality of a particular event, we calculated the distance between the actual position of the first spark in the exit spark chamber and the expected position (estimated by extrapolation from the focal-plane wire chamber). Another quantity,  $\chi_x^2$ , was used in assessing the event reconstruction. This was defined as the square of the difference (measured in units of the expected deviation) between the actual location of the sparks at the focal plane and the location predicted according to the entrance wire chamber addresses and the calculated momentum.

If one of the focal-plane wire chambers failed to report, its address was constructed by an extrapolation from the wire chamber that did report to the first spark in the exit spark chamber. If neither focal-plane chamber reported, the reconstruction was made by using the path of the track as observed in the exit chamber. All such reconstructions were noted on the output tape. For those events with more than one possible set of initial or final conditions, all possible combinations were formed and the set with the minimum  $\chi_x^2$  was chosen.

The resultant reconstruction for each event was then subject to a final reduction by a variety of requirements, which are discussed in Sec. IV.

### III. MONTE CARLO CALCULATION

The procedure of the analysis was to compare the final data with distributions generated by a Monte Carlo calculation and determine the relative number of events for each mode with respect to the number of  $K_{\mu 2}$ . The routine was designed to simulate events and to analyze these events with the data-reduction programs. Decay events with initial momenta randomly generated from their respective theoretical momentum distributions were tracked by the orbit-tracking program through the system. The energy loss, straggling, and scattering were calculated for the hypothetical particle passing through the various pieces of material along the trajectory. For electrons, radiation and corrected ionization losses were included.<sup>30-32</sup>

The decay in flight and nuclear absorption of the pions were also simulated. In the case in which the mock pion had decayed (via  $\pi \rightarrow \mu + \nu$ ) in flight from the target to the exit spark chamber, the trajectory of the resultant muon was followed to the end of its range. Pion nuclear absorption was determined by using experimentally measured cross sections for nuclear inter-

<sup>30</sup> L. Landau, *J. Phys. Radium* **8**, 201 (1944).

<sup>31</sup> W. Heitler, *The Quantum Theory of Radiation* (Oxford University Press, New York, 1954), 3rd ed.

<sup>32</sup> R. R. Wilson, *Phys. Rev.* **84**, 100 (1951).

actions of pions in various materials, including large-angle scattering and production of stars.<sup>33,34</sup> The wire chamber crossing positions, the counters that fired, and the positions of the first and last sparks in the exit spark chamber were generated, and this information was then processed by the data-analysis programs.

The scanning of the exit chamber included as primary tracks those decays which occurred within  $10^\circ$  of the initial particle direction. This bias was also included by calculation of the trajectory of the electron resulting from pion and muon decay at rest. The efficiency of the focal-plane wire chambers as a function of momentum was included by folding the efficiency (see Fig. 5) into the momentum distributions for the different modes, correcting for the fraction of reconstructed events.

Figure 6 shows four comparisons of the data with the Monte Carlo results. Plot I is a distribution of the length of  $K_{\mu 2}$  muon tracks in the exit chamber. Plot II is the distribution of deviation of the first spark in the exit chamber from the projection using the focal-plane wire chambers. Plots III and IV are distributions of particle initial position and angle, respectively, as projected from entrance wire chamber addresses. The value of  $\chi^2$  divided by the number of degrees of freedom for these

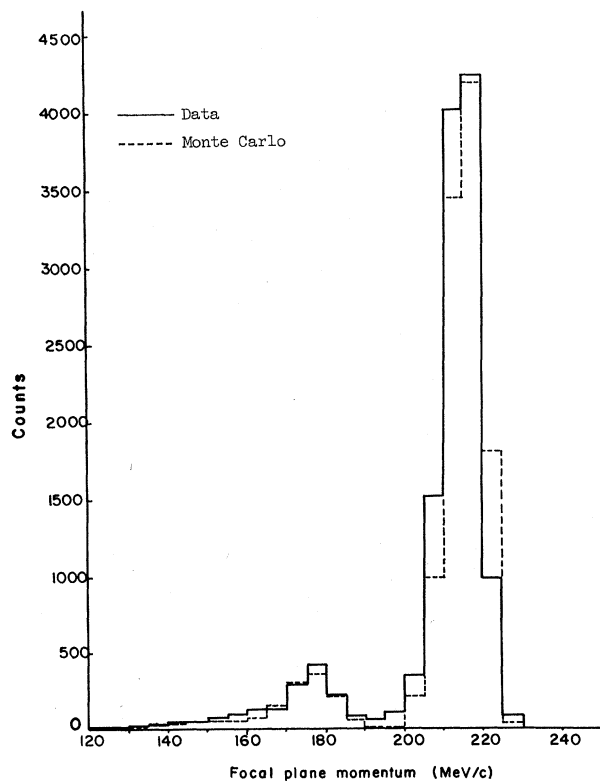


FIG. 7. Momentum spectrum as seen at the focal plane (solid line, data; dashed line, calculated histogram).

<sup>33</sup> J. F. Tracy, Phys. Rev. **91**, 960 (1953).

<sup>34</sup> C. Chedester, P. Isaacs, S. Sachs, and J. Steinberger, Phys. Rev. **82**, 958 (1951).

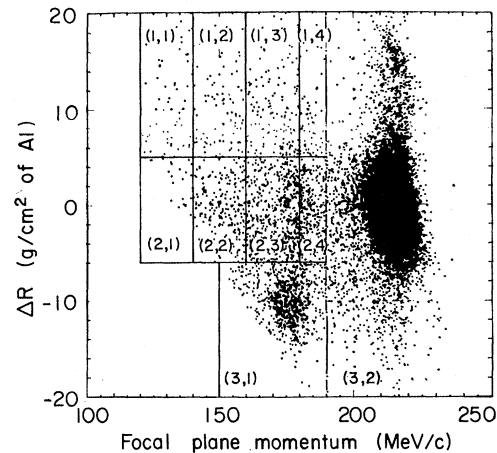


FIG. 8. Data scatter plot.

plots are 1.19, 1.99, 1.07, and 0.84, respectively. These particular distributions display the ability of the Monte Carlo calculation to simulate data. Plots I and II reflect the orbit tracking, while plots III and IV indicate the acceptance by the spectrometer.

#### IV. DATA SAMPLE AND GATE REQUIREMENTS

The final data sample consists of 18 000 events in the momentum interval 120–240 MeV/c. The momentum distribution at the focal plane is compared with the Monte Carlo calculation in Fig. 7.

In Fig. 8 the data are shown as a two-dimensional plot of momentum versus difference between the observed range and the muon range for that momentum. In this plot muons appear in a horizontal band about  $\Delta R=0$ , and pions appear in an approximately horizontal band about  $\Delta R=10.0$  g/cm<sup>2</sup>; electrons have no definite range.

The data shown in Figs. 7 and 8 have been selected to satisfy various criteria that serve to remove background and ambiguous events. The selection requirements were chosen to minimize any biases that might depend on the mode of decay. The events generated by the Monte Carlo calculation were subject to the same selection requirements. These included a lower limit (approximately 15 nsec) on the decay-time distribution to eliminate  $K^+$  decay in flight and prompt pions scattering into the apparatus, an upper limit on  $\chi^2$  to minimize the number of events reconstructed from accidental wire addresses, and limits on the initial conditions of events to ensure physically reasonable trajectories. Figure 9 shows the above distributions with their respective limits of acceptability.

Approximately 30% of the data included events for which  $K^+$  lifetime information was lacking. Correction was made for the events which in fact would miss the decay-time gate by subtracting a distribution of events with lifetime information but falling outside the time

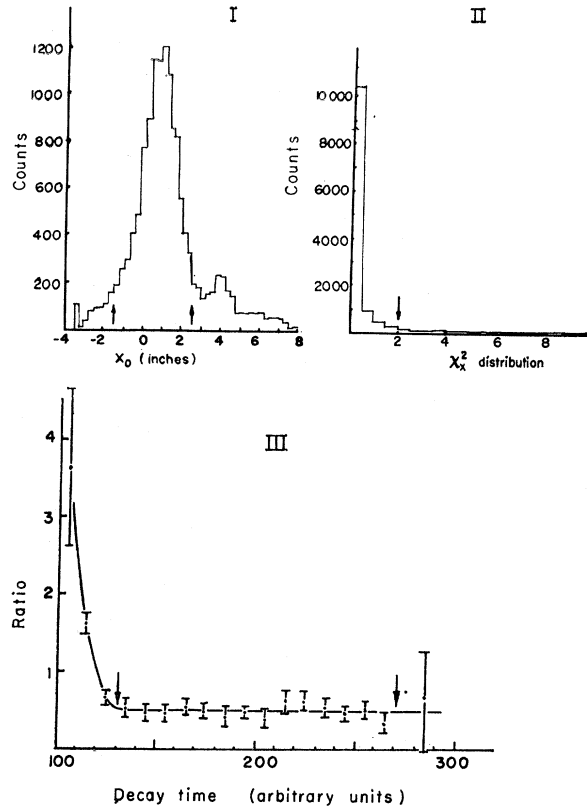


FIG. 9. Distributions with gates. (I) Initial spatial distribution. (II)  $\chi^2$  distribution. (III) Ratio of events below 190 MeV/c to events above versus decay time.

gates; the distribution was scaled by the ratio of total events without time information to the total number with time information. After allowance for the fraction of events which would miss the time gate the net contribution was 24% to the final data array.<sup>35</sup>

## V. FINAL ANALYSIS

### A. Background Subtraction

There are three major sources of background:  $K^+$  decay in flight,  $\pi^+$  scattering out of the beam into the apparatus, and events coming from sources other than the target. The decays in flight and the scatterings occur as prompt events with respect to the arrival of a trigger in the beam telescope and thus can be made negligible by adjustment of the lower limit on the decay time.

The remaining background was removed by a subtraction from the data. Comparison of the momentum spectrum of events originating from the target with that of events whose projected initial position is outside the target [see Fig. 9(I)] shows that there are significantly more off-target events with momentum below the  $K_{\mu 2}$  region. Explicitly, the ratio of events below 190 MeV/c

to total events is  $(14.8 \pm 1.1)\%$  for events originating inside the target volume and  $(31.0 \pm 2.5)\%$  for events originating outside. The larger fraction of low-momentum events results from an increase in material through which these particles pass, and the only such material is the  $\gamma$ -ray spark chamber positioned about the target. The  $K^+$ 's in the beam scatter out of the stopping region and stop in the plates of these chambers. The scattered  $K^+$ 's that decay from these plates are distributed nearly uniformly over the faces of the chambers, and some decay trajectories pass through the target volume. These events are indistinguishable from normal events in which the  $K$  stopped in the target; however, their momentum is reduced.

The range-momentum distribution of the background was made by a Monte Carlo calculation assuming the scattered  $K^+$ 's to be uniformly distributed over the face of the chambers. The stopping positions in the brass were determined by using experimental range curves. The resultant range-momentum array (see Fig. 10) was normalized to the data by the fraction of background events under the peak of the initial position distribution. A straight-line fit to the data outside the peak of Fig. 9(I) was made. The number of events under this line that met the selection criteria was then used as the number of background events. The normalized background was subtracted from the data range-momentum plot.

### B. Method

The branching ratio was finally determined by an analysis of the two-dimensional range-momentum scattergrams. These scattergrams were divided into regions or cells as shown in Fig. 8. This cell structure was chosen so that the majority of events could be classified as follows:

- cells (1,1) and (1,2):  $K_{e3}$  electrons;
- cell (3,2) :  $K_{\mu 2}$  muons;
- cells (2,1) and (2,2):  $K_{\mu 3}$  muons;
- cell (3,1) :  $K_{\pi 2}$  pions;
- cells (2,3) and (2,4):  $K_{\pi 2}$  muons from decay in flight and at rest, background from  $K_{\mu 2}$  muons origi-

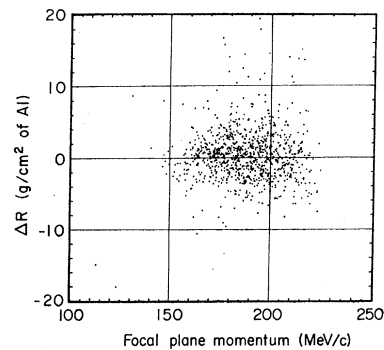


FIG. 10. Scatter plot of background calculation.

<sup>35</sup> N. T. Dairiki, University of California Lawrence Radiation Laboratory Report No. UCRL-18245 (unpublished).

TABLE II. Summary of uncertainties and errors (%).

	Sources of errors			
	$K_{\mu 2}$	$K_{\pi 2}$	$K_{\mu 3}$	$K_{e3}$
Statistical fluctuation: data	$\pm 0.8$	$\pm 3.0$	$\pm 6.3$	$\pm 5.8$
Statistical fluctuation: Monte Carlo	$\pm 1.0$	$\pm 1.5$	$\pm 3.5$	$\pm 3.5$
Tracking program <sup>a</sup>	$\pm 3.0$	$\pm 3.0$	$\pm 3.0$	$\pm 3.0$
Location of pieces of apparatus <sup>a</sup>	0.0	0.0	$\pm 1.0$	$\pm 1.0$
Pion nuclear absorption cross sections <sup>a</sup>		$\pm 1.4$		
Energy-loss calculations	$\pm 0.8$	$\pm 2.5$	$\pm 0.8$	$\pm 1.0$
Electron scattering				$\pm 3.0$

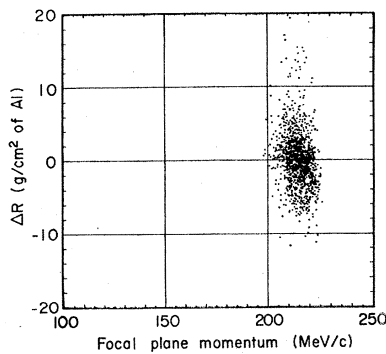
<sup>a</sup> These errors do not affect  $\Gamma(K_{\mu 3})/\Gamma(K_{e3})$ .

nating from within the plates of the brass spark chambers, and  $K_{\mu 3}$  muons.

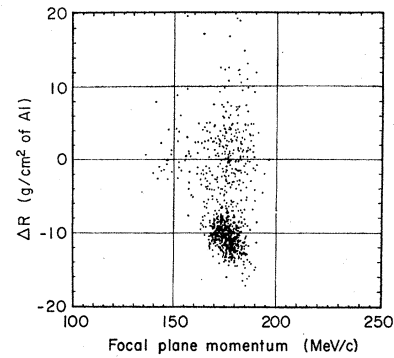
The  $\tau$  and  $\tau'$  modes of decay ( $K^+ \rightarrow \pi^+\pi^-\pi^+$  and  $K^+ \rightarrow \pi^+\pi^0\pi^0$ ) were excluded from the system due to insufficient range of the decay pions. To determine the relative branching ratios  $R_i = \Gamma_i/\Gamma(K_{\mu 2})$ , with  $i = K_{\pi 2}, K_{\mu 3}, K_{e3}$ , a  $\chi^2$  function was constructed comparing the calculated and experimental data distributions on a cell-by-cell basis, and the  $\chi^2$  was minimized.<sup>36</sup> The uncertainties included in the formation of the  $\chi^2$  function were those due to statistical uncertainties in the data and the Monte Carlo calculation and the uncertainty in the focal-plane wire chamber efficiency. In addition, instrumental uncertainties and possible systematic errors, presented in Table II, were added to the errors resulting from the  $\chi^2$  minimization routine.

### C. Results

The range-momentum scatter plot for the final data sample is shown in Fig. 8, along with the division into bins. The calculated distributions for the four modes measured in this experiment are shown in Figs. 11–14. The background calculation is shown in Fig. 10. Table III shows the data array after background subtraction, the input to the  $\chi^2$  program for each mode, normalized

FIG. 11. Scatter plot of  $K_{\mu 2}$  Monte Carlo calculation.

<sup>36</sup> J. Orrear, University of California Lawrence Radiation Laboratory Report No. UCRL-8417, 1957 (unpublished).

FIG. 12. Scatter plot of  $K_{\pi 2}$  Monte Carlo calculation.

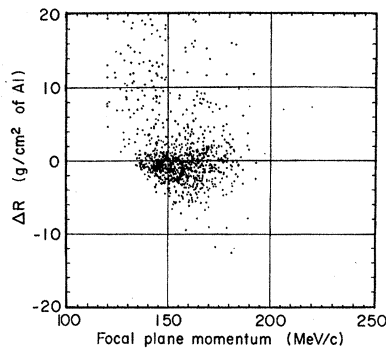
and corrected for chamber inefficiencies, and the resulting composite array from the  $\chi^2$  minimization. The branching ratios calculated as relative rates normalized to the  $K_{\mu 2}$  cell are  $K_{\mu 2} = 0.997 \pm 0.015$ ,  $K_{\pi 2} = 0.304 \pm 0.017$ ,  $K_{\mu 3} = 0.054 \pm 0.009$ , and  $K_{e3} = 0.069 \pm 0.006$ . The errors include statistical and systematic uncertainties as shown in Table II.

The reason the  $K_{\mu 2}$  is not identically 1.000 is that a small amount of  $K_{\mu 2}$  muons extend beyond the (3,2) cell (see Table III). The actual normalization is to this cell, and the  $K_{\mu 2}$  ratio is then evaluated along with the other branching ratios.

When one uses the accepted branching ratios for the three-pion modes,  $\tau' = (1.71 \pm 0.07)\%$  and  $\tau = (5.57 \pm 0.03)\%$ ,<sup>37</sup> the branching ratios become  $K_{\mu 2} = (65.0 \pm 0.9)\%$ ,  $K_{\pi 2} = (19.8 \pm 1.1)\%$ ,  $K_{\mu 3} = (3.5 \pm 0.6)\%$ , and  $K_{e3} = (4.4 \pm 0.4)\%$ . Comparison of the composite range-momentum plot for the Monte Carlo calculation with the data array, using the above branching ratios, yields a  $\chi^2$  of 8.77 for six degrees of freedom.

From the above one has

$$\Gamma(K_{\mu 3})/\Gamma(K_{e3}) = 0.81 \pm 0.13,$$

FIG. 13. Scatter plot of  $K_{\mu 3}$  Monte Carlo calculation.

<sup>37</sup> A. H. Rosenfeld, A. Barbaro-Galtieri, J. Kirz, W. J. Podolsky, M. Ross, W. J. Willis, and C. G. Wohl, University of California Lawrence Radiation Laboratory Report No. UCRL-8030 (rev.), 1966 (unpublished).

TABLE III. Range-momentum arrays ( $\Delta R$  in  $\text{g}/\text{cm}^2$  Al).

$P$ (MeV/c)	120-139	140-159	160-179	180-189	190-235
Range-momentum array: numbers of events (data minus background)					
$20.0 \geq \Delta R \geq 5.0$	$106.2 \pm 10.9$	$134.5 \pm 12.5$	$177.1 \pm 18.2$	$51.5 \pm 13.9$	$15\,208.0 \pm 154.0$
$5.0 \geq \Delta R \geq -6.0$	$26.7 \pm 5.7$	$252.3 \pm 17.9$	$448.4 \pm 49.5$	$99.4 \pm 59.0$	
$-6.0 \geq \Delta R \geq -20.0$			$1002.0 \pm 33.6$		
Range-momentum array: Monte Carlo (arbitrary normalization)					
			$K_{\mu 2}$		
		0.13	0.13	0.56	556.44
			0.52	1.26	
			0.82		
			$K_{\pi 2}$		
	0.57	1.28	10.15	5.57	3.87
		13.18	37.47	15.26	
			117.58		
			$K_{\mu 3}$		
	7.07	5.43	3.03	0.55	0.95
	13.93	72.18	49.72	4.95	
			1.16		
			$K_{e 3}$		
	46.76	68.62	39.05	7.48	3.48
	4.68	12.81	10.96	1.34	
			1.71		
Monte Carlo results scaled by branching ratios and summed					
	95.9	144.0	163.7	75.9	15 204.5
	33.8	242.6	418.3	170.7	
			1002.5		

which gives the form-factor ratio

$$\xi(0) = 0.91 \pm 0.82,$$

assuming  $\lambda_+ = 0.023$  and  $\lambda_- = 0.0$ .

The momentum distribution of the  $K_{\mu 3}$  mode was generated for both  $\xi(0) = 0$  and  $\xi(0) = 1.0$ . These two spectra were compared with the data and both yielded the same value of  $\Gamma(K_{\mu 3})/\Gamma(K_{e 3})$  to within the statistical significance of the experiment. The result of the measurement of the  $K_{\mu 2}/K_{\pi 2}$  ratio is

$$\Gamma(K_{\mu 2})/\Gamma(K_{\pi 2}) = 3.28 \pm 0.18.$$

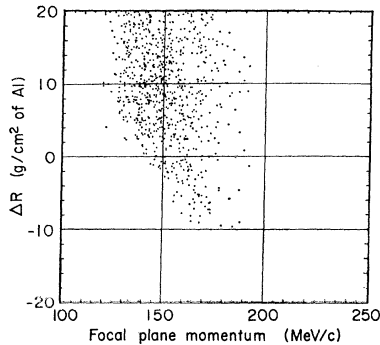


FIG. 14. Scatter plot of  $K_{e 3}$  Monte Carlo calculation.

#### D. Conclusion

As seen in Fig. 1, our results are in agreement with most previous measurements; in particular, we show agreement with other spectrometer experiments.<sup>11,14,15</sup> Our results may also be compared with others by examining the various values of  $\xi(0)$  as shown in Fig. 2. All of the points included in the determination of  $\xi(0)$  from branching-ratio measurements have been calculated assuming  $\lambda_- = 0.0$  and using the branching ratios quoted by the various authors. The  $\chi^2$  for these points with respect to the weighted average of  $-0.03 \pm 0.11$  is 22.3 for nine degrees of freedom. This leads to a confidence level of 0.6%, which reflects the fact that the fluctuations due to systematic uncertainties exceed those expected from statistics.

We note, however, that of the nine experiments shown in Fig. 2, all but two (5,13) yield values of  $\xi(0)$  which deviate from the value as determined by polarization measurements by more than 2 standard deviations. We also note that the most significant of these two measurements (13) deviates in  $\Gamma(K_{\mu 3})/\Gamma(K_{e 3})$  from both the world averages of this ratio for  $K^0$  and  $K^+$  decays by more than 3 standard deviations.

As mentioned in the Introduction, it has been suggested that a large momentum-transfer dependence of the form factors may be used to reconcile the differences between the values of  $\xi(0)$ . Since  $\lambda_+$  has been experi-

mentally determined ( $\lambda_+ = 0.023 \pm 0.008$ ), the only term available to yield such a dependence is  $f_-(q^2) = f_-(0)(1 + \lambda_- q^2/m_\pi^2)$ . However, since the maximum value of  $q^2/m_\pi^2$  is 6.7, we feel that values of  $|\lambda_-|$  greater than 0.2 would contradict the assumption that  $f(q^2)$  is a slowly varying function of  $q^2$ . We also refer to Cutts,<sup>38</sup> who places a 2-standard-deviation limit of  $\lambda_- > -0.2$  from a  $K_{\mu 3}$  polarization measurement. A third consideration in placing this limit is that a value of  $|\lambda_-|$  greater than 0.2 indicates the resonance mass propagating the interaction to be considerably less than  $M_K$ . A  $|\lambda_-|$  of this size is also larger than any present theoretical predictions. If we use the value of  $\lambda_- = -0.2$  in determining  $\xi(0)$  from the branching-ratio measurements, the result is  $\xi(q^2=0, \lambda_- = -0.2) = -0.50 \pm 0.15$ . This value is still in disagreement with the polarization measurements. From Cutts<sup>38</sup> we see that a strong momentum-transfer dependence of the form factors will not alter the polarization value of  $\xi(0)$  in a way to bring it into agreement with the branching-ratio value.

We have compiled further data pertaining to different determinations of  $\xi(0)$ . These data, results of measurements of the  $\mu^+$  momentum spectrum,  $\pi^0$  momentum spectrum,  $\pi^0$ - $\mu^+$  angular correlations, and  $\mu^+$  Dalitz-plot measurements, are shown in Table IV.<sup>39-43</sup> The weighted average of  $\xi(0)$  from these measurements is  $\xi(0) = 0.45 \pm 0.26$ . Again, we realize that the differences among these data are larger than one would expect from statistical fluctuations alone; however, we must point out that the weighted average is in disagreement with a value of  $\xi(0) = -1.0 \pm 0.2$ .

In summary, except for the polarization measurements, we can find only one experiment (13) which is inconsistent to 2 standard deviations with a value of  $\xi(0) = -0.03 \pm 0.11$ . On the other hand, we find nine experiments which yield values of  $\xi(0)$  differing by more

TABLE IV. Other determinations of  $\xi(0)$ .

Method	Re $\xi(0)$ <sup>a</sup>	Im $\xi(0)$	Reference
$\mu^+$ spectrum	$0.0_{-0.9}^{+1.1}$	$0.0 \pm 1.0$	Callahan, 1966 <sup>b</sup>
$\pi^0$ spectrum	$0.72 \pm 0.37$	Assume 0	Callahan, 1966 <sup>b</sup>
$\pi^0$ - $\mu^+$ angular correlation			
$\mu^+$ spectrum	$-1.2 \pm 1.0$	$ \text{Im}\xi(0)  < 2.4$	Jenson, 1965 <sup>c</sup>
$\mu^+$ spectrum	$0.7 \pm 0.5$	Assume 0	Giacomelli, 1964 <sup>d</sup>
$\mu^+$ spectrum	$+1.8 \pm 1.6$	Assume 0	Brown, 1962 <sup>e</sup>
$K_{\mu 3}^+$ Dalitz plot	$-0.5 \pm 0.9$	2.3	Eisler, 1968 <sup>f</sup>
$K_{\mu 3}^0$ Dalitz plot	$+1.2 \pm 0.8$	Assume 0	Carpenter, 1966 <sup>g</sup>

<sup>a</sup> Weighted average Re $\xi(0) = 0.45 \pm 0.26$ .

<sup>b</sup> Reference 9.

<sup>c</sup> Reference 39.

<sup>d</sup> Reference 40.

<sup>e</sup> Reference 41.

<sup>f</sup> Reference 42.

<sup>g</sup> Reference 43.

than 2 standard deviations from  $\xi(0) = -1.0 \pm 0.2$ . From this evidence we must conclude that the polarization measurements are in disagreement with the bulk of the data from other sources. This lack of agreement may be due to undetected systematic errors in the polarization and/or other experiments, or to an error in the assumptions leading to the phenomenology describing  $K$ -meson decays (i.e., possibly a lack of  $\mu$ - $e$  universality as suggested by Stiening<sup>44</sup>).

Further experimentation is needed, but such experiments should be capable of detecting inconsistencies in the phenomenology and should be significantly different from previous experiments to minimize the effects of systematic errors.

#### ACKNOWLEDGMENTS

We thank the staff of the Lawrence Radiation Laboratory for their assistance throughout all phases of the experiment. Most notably we thank R. Fulton, R. Peters, and K. Mirk of the Mechanical Engineering Department, L. Proehl and F. Kirsten of the Nuclear Instrumentation Department, and the operating crew of the Bevatron. We also acknowledge the help of Dr. P. Steinberg during the running of the experiment, and of the scanning staff, especially P. Craig and J. Bistirlich, during the analysis phase.

<sup>44</sup> R. F. Stiening, University of California Lawrence Radiation Laboratory Report No. UCRL-18231, 1968 (unpublished) (presented as invited paper, Washington APS meeting, 1968).

<sup>38</sup> D. Cutts, University of California Lawrence Radiation Laboratory Report No. UCRL-18143, 1968 (unpublished).

<sup>39</sup> G. L. Jensen, C. T. Murphy, and B. P. Roe, Phys. Rev. **138**, B1507 (1965).

<sup>40</sup> G. Giacomelli, D. Monti, G. Quarenzi, A. Quarenzi-Vignudelli, W. Puschel, and J. Tietge, Nuovo Cimento **34**, 1134 (1964).

<sup>41</sup> J. L. Brown, J. A. Kadyk, G. H. Trilling, R. T. Vande Walle, B. P. Roe, and D. Sinclair, Phys. Rev. Letters **8**, 450 (1962).

<sup>42</sup> F. R. Eisler, S. Y. Fung, S. L. Marateck, S. L. Meyer, and R. J. Plano, Phys. Rev. **169**, 1090 (1968).

<sup>43</sup> D. W. Carpenter, A. Abashian, R. J. Abrams, G. P. Fisher, B. M. K. Nefkens, and J. H. Smith, Phys. Rev. **142**, 871 (1966).